



Arginine-rich peptide based nanoparticles with bridge-like structure: Enhanced cell penetration and tumor therapy effect



Xinxin Yan^{a,b}, Lin Lin^c, Shengran Li^{a,b}, Wenliang Wang^d, Binggang Chen^{a,b}, Sangni Jiang^{a,b}, Sanrong Liu^{a,*}, Xiaojing Ma^{a,*}, Xifei Yu^{a,b,*}

^a Laboratory of Polymer Composites Engineering, Changchun Institute of Applied Chemistry, Chinese Academy of Sciences, Changchun, Jilin 130022, China

^b University of Science and Technology of China, Hefei, Anhui 230026 China

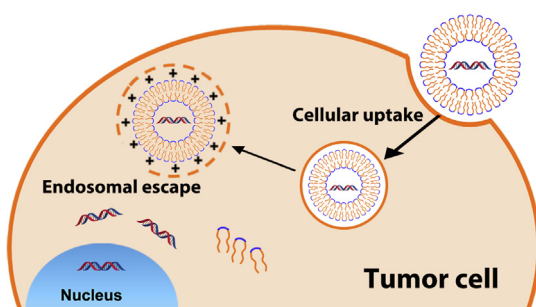
^c Laboratory of Polymer Ecomaterials, Changchun Institute of Applied Chemistry, Chinese Academy of Sciences, Changchun, Jilin 130022, China

^d Department of Neurology, Johns Hopkins University School of Medicine, Baltimore, MD 21205, USA

HIGHLIGHTS

- An arginine-rich peptide as gene vectors.
- The fluorous chains conferred anti-serum capability.
- The bridge-like peptide enhanced cellular uptake efficiency.
- Good tumor targeting ability and strong anti-tumor effects.

GRAPHICAL ABSTRACT



ARTICLE INFO

Keywords:

Arginine
Cell penetrating peptides
Bridge-like
Tumor therapy

ABSTRACT

Gene therapy has been recognized as one of the most potential approaches on cancer treatment field. Arginine-rich cell penetrating peptides have attracted enormous interests in gene delivery field due to their superior membrane translocation capability. Herein, we developed a novel arginine-rich peptide based gene delivery system consisted of tri-block copolymers C₇F₁₅-R(HR)₅K-C₇F₁₅. The tri-block copolymers would assemble into nanoparticles in aqueous solution with special bridge-like structure denoted as NPT. At the same time, di-block copolymers Ac-R(HR)₅K-C₇F₁₅ were constructed and assembled into nanoparticles named NPD as control. The bridge-like structure extremely promoted interaction efficiency of arginine residues and cell membrane leading to enhanced endocytosis and gene transfection efficiency. Compared with NPD of traditional structure, NPT exhibited superior in vitro gene transfection efficiency which was two fold higher than NPD. Anti-epidermal growth factor receptor (EGFR)-shRNA loaded NPT caused 95% apoptosis of MCF-7 cells and significant tumor inhibition effect with neglected toxicity. These may help NPT step forward to further application.

1. Introduction

Gene therapy is regarded as one of the most potential approaches on treating cancer disease through delivering therapeutic genes into cancer

cells and regulating abnormal genes without damage to normal parts [1–3]. Epidermal growth factor receptor (EGFR) is a kind of over-expressed protein on many cancer cells and highly related to the proliferation and migration of cancer cells [4]. Previous work have proved

* Corresponding authors.

E-mail addresses: xjma@ciac.ac.cn (X. Ma), xfyu@ciac.ac.cn (X. Yu).

using anti-EGFR genes to knock down the expression of EGFR could efficiently inhibit the tumor growth efficiently [5]. However, as negative charged macromolecules, nucleic acids are unable to cross negative charged cell membrane and internalize cancer cells by themselves [6,7]. To ensure the therapy effect, researchers have designed and synthesized various gene delivery systems to promote the internalization efficiency of therapeutic nucleic acids. With the development of gene carriers, cationic polymers have gained enormous investigation due to its superior transfection efficiency [2,8,9]. The high positive charge carried by cationic polymers conferred them high binding affinity with nucleic acids and strong interactions with biological membranes, which attributed to the high transfection efficiency. While high positive charges bring fatal problems-cationic-related toxicity [10,11]. The contradiction between high efficiency and biosafety severely limited the clinical application of cationic polymers [12]. Therefore, a gene delivery system with both high efficiency and safety is still in urgent demand.

Decades ago, scientists found a variety of short cationic peptides named cell penetrating peptides (CPPs). The attachment of CPPs to other molecules could efficiently enhanced cellular internalization with a manner of low cytotoxicity [6,13,14]. This special characteristic conferred CPPs huge application potential in gene therapy field and related study increased rapidly [15,16]. The deep study about penetrating mechanism indicated that special characteristic of CPPs was highly related to the arginine residues rich in the CPPs [17,18]. The guanidine groups of arginine could form bidentate hydrogen bonds and ion pairs with phosphate moieties on cell membrane, leading to enhanced internalization [19]. Therefore, a lot of synthetic arginine-rich peptides were developed and investigated [20,21]. Tang etc. introduced poly(arginine) mimics into DNA delivery system and promoted the cell membrane permeability significantly [20]. Tai developed a cationic arginine-rich polypeptide and demonstrated the high efficacy in siRNA delivery [22]. The excellent cell internalizing effect of arginine has gotten well confirmed in these researches. But we found that in most applications, those functional arginine-rich peptides were present in a flexible linear manner conjugated to delivery systems and led to limited interaction of guanidine groups with cell membrane [23–25]. Considering the internalizing mechanism of arginine residues, excessive arginine residues would be needed to ensure final cell penetrating effect [26,27]. However, the pKa of guanidine group is approximately 12.5 and excessive arginine groups would exhibit highly basic. It means the introduction of traditional arginine-rich CPPs could not avoid cationic-related toxicity completely though cellular internalizing efficiency got promoted compared with other typical cationic polymers. Gisela and his team cyclized R10 and found the membrane contacts increased leading to enhanced cell penetration [28]. In another hand, Paul A. Wender and his team found that increasing backbone spacing of arginine-rich transporters would facilitate cell uptake efficiency [29]. Hence, improving membrane contact efficiency to achieve enhanced internalizing efficiency with less arginine residues would be a promising way to solve the contradiction between toxicity and efficiency. It also should be noted that positive charge carried by arginine residue can adsorb serum protein and form protein corona in physiological environment. The protein corona will influence bioactivity and therapy effect of delivery systems [30,31]. To decrease formation of protein corona, fluorous compounds could be introduced attributed to their hydrophobic and lipophobic features.

Inspired by these points, we designed and synthesized a novel arginine-rich peptide based gene delivery system shown with bridge-like structure as shown in **Scheme 1a**. The functional peptide with sequence of RHRHRHRHRHK was conjugated with perfluoroctanoyl fluoride chains each side to form tri-block copolymer. This amphiphilic copolymer could assemble into spherical hollow nanoparticles in aqueous solution denoted as NPT. The existence of hydrophobic fluorous chains at two ends made functional peptide form bridge-like structure. Obviously the bridge-like structure could extremely promote the

membrane interaction efficiency of each guanidine group when NPT contacts cell membrane. Meanwhile, the increased backbone rigidity and expanded distance between guanidine groups further promote cell membrane interaction [29,32]. Enhanced cell membrane interaction ensures cell internalization efficiency with less arginine residues. The histidine inserted between arginine residues could protonate in acid environment, induce endosome lysis and help releasing loaded DNA into cytoplasm after entering cells [33,34]. The fluorous chains at two ends are both hydrophobic and lipophobic [35–37]. This property makes system more stable to serum components leading to prolonged circulation time in physiological fluids. These outstanding characteristics would make NPT a promising gene delivery system.

2. Experimental

2.1. Materials

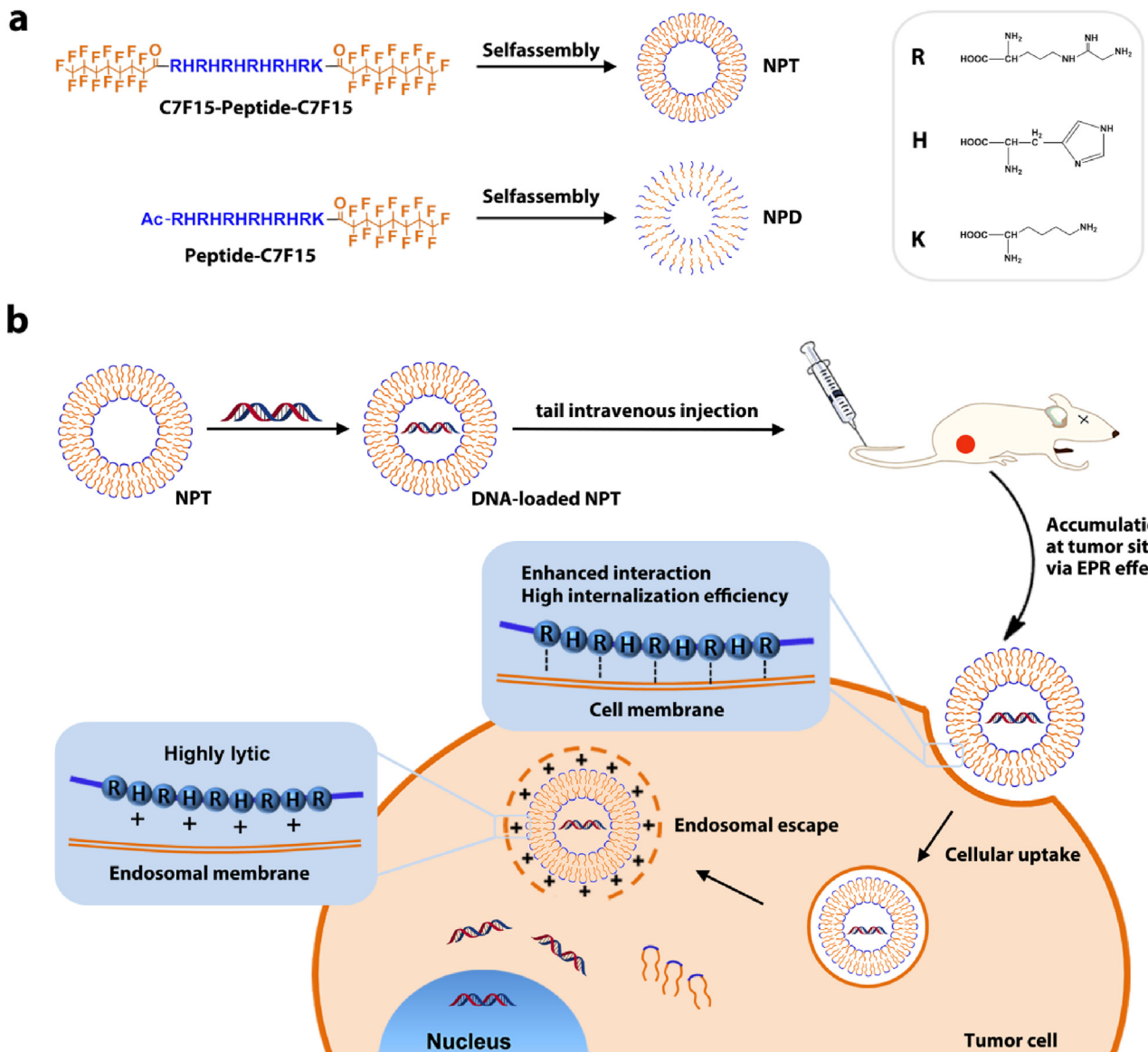
Two kinds of polypeptides ($\text{NH}_2\text{-R-H-R-H-R-H-R-H-R-K-COOH}$, Mw = 1768.03; $\text{Ac-R-H-R-H-R-H-R-H-R-K-COOH}$, Mw = 1768.03) were purchased from YuanPeptide Biotech Ltd (Nanjing, China). Perfluoroctanoyl chloride was purchased from Alfa (Shanghai, China). Branched poly(ethelyimine) (25 kD) (BPEI 25 K) and 4',6-diamidino-2-phenylindole (DAPI) were purchased from Sigma (Sigma-Aldrich, St. Louis, MO, USA). LysomeTracker dye was purchased from Best Bio (Nanjing, China). Cy5 DNA was obtained from Ribo Bio (Guangzhou, China). Anti-epidermal growth factor receptor (EGFR)-shRNA and siRNA genes (sense strand: 5'-GGCUGGUUAUGUCCUCAUU dTdT-3'; antisense strand: 3'-dTdT CCGACCAAUACAGGAGUAA-5') and plasmid expressing green fluorescent protein (pGFP) were purchased from Genepharma Company (China). All plasmids were amplified in Escherichia coli and purified with Endo-free Plasmid Maxi Kit supplied by Tiangen biotech (Beijing, China). Stable transferred HeLa cells were supplied by Golden Trans Technology (Changchun, China). Cell titer-blue cell viability assay was purchased from Promega (Madison, WI). Annexin V-fluorescein isothiocyanate (FITC)/propidium iodide (PI) apoptosis detection kit was purchased from keyGEN BioTECH (China). RPMI-1640 medium, 0.25 wt% trypsin with 0.02 wt% ethylenediaminetetraacetic acid, fetal bovine serum (FBS), streptomycin, and penicillin were purchased from Gibco BRL (USA).

2.2. Synthesis of tri-block and di-block copolymer

To synthesize tri-block copolymer, polypeptides ($\text{NH}_2\text{-RHRHRHRHK-COOH}$, 10 mg), perfluoroctanoyl chloride (4 μL) and triethylamine (5 μL) were added into dimethyl sulfoxide (DMSO) (5 mL) and dissolved absolutely. Then the mixture was stirred for 24 h at room temperature. After reacting for 24 h, the solution was collected and dialyzed (Molecular Weight Cut Off 1000) in ultrapure water to remove excess perfluoroctanoyl chloride and triethylamine. Tri-block copolymer was finally obtained through lyophilization. Di-block copolymer was synthesized by the same procedure as tri-block copolymer.

2.3. Preparation and characterization of NPT, NPD, NPT/DNA and NPD/DNA

Tri-block copolymer and di-block copolymer were dissolved in ultrapure water individually (1 mg/mL) under ultrasonic for 30 min. Then the solution was filtrated with filters (200 nm) and placed for 2 h to get NPT/NPD solution. The morphology, surface charge and size distribution were measured by TEM and Zetasizer (Malvern). The DNA-loaded NPT/NPD were prepared as following: tri-block copolymer or di-block copolymer solution (1 mg/mL) was sonicated for 1 min and then mixed with DNA at different nitrogen/phosphorus (N/P) ratios. Still, the morphology, surface charge and size distribution of DNA-loaded NPT/NPD were measured by TEM and Zetasizer.



Scheme 1. The working mechanism of NPT as gene delivery system. (a) Detailed structure design of NPT and NPD. (b) The process of NPT to transport DNA into tumor cells and escape from endosomes.

2.4. Gel electrophoresis assay

Gel electrophoresis assay was performed to evaluate the binding affinity of NPT and NPD. Commercial transfection agent BPEI 25 K was used as positive control. NPT, NPD and BPEI 25 K were complexed with DNA at N/P ratio of 0, 1, 2, 3, 4 and 5 and incubated for 30 min at room temperature. All the samples were mixed with loading buffer and electrophoresed in 1 × Tris-acetate-EDTA (TAE) buffer at 120 V for 40 min. DNA bands were observed by a Gel Doc XR image analyzer.

2.5. Cellular uptake and intracellular DNA distribution study

To evaluate the cell uptake efficiency of NPT and NPD, MCF-7 cells were seeded on glass-bottom petri dishes with 8×10^4 cells and incubated overnight. Fresh RPMI 1640 medium containing Rhodamine B-loaded NPT/NPD was added respectively to incubate cells for 1 h when cell confluence reached 60%-70%. Concentrations of NPT and NPD were both 5.0 mM. After 1 h, cells were washed with PBS gently three times and observed with confocal lazer scanning microscope (CLSM, LSM 700 Carl Zeiss Microscopy). To determine the subcellular location

of DNA-loaded NPT/NPD, MCF-7 cells (8×10^4 cells per dish) were seeded on glass-bottom petri dishes. After cell confluence reached 70%, the old medium was replaced by fresh RPMI 1640 medium containing BPEI 25 K/Cy5 DNA complex, Cy5 DNA-loaded NPD and Cy5 DNA-loaded NPT. Cy5 DNA was added at 2 $\mu\text{g}/\text{dish}$ and N/P ratio was 10. After incubation for 2 h, the cells were washed with PBS for three times and fixed with 4% formaldehyde for 30 min. The lysome was stained with LysomeTracker (75 nM) for 1 h and then the nucleus was stained with DAPI (10 $\mu\text{g}/\text{mL}$) for 10 min. To evaluate of DNA-loaded NPT/NPD cellular uptake efficiency, CLSM and flow cytometry (BD Biosciences) were conducted at the same time. For Confocal analysis, MCF-7 cells (8×10^4 cells per dish) and HeLa cells (7×10^4 cells per dish) were seeded on glass-bottom petri dishes individually. When cell confluence reached 60%-70%, the old medium was removed and RPMI 1640 medium containing Cy5 DNA-loaded NPT/NPD was added to incubate cells for 1 h and 4 h. Cy5 DNA was added at 2 $\mu\text{g}/\text{dish}$ and N/P ratio was 10. After incubation time, cells were washed with PBS and fixed with 4% formaldehyde for 30 min and stained with DAPI (10 $\mu\text{g}/\text{mL}$) for 8 min at 37°C. The prepared samples were observed with CLSM. For flow cytometry, MCF-7 cells (7×10^4 cells per well) and HeLa cells

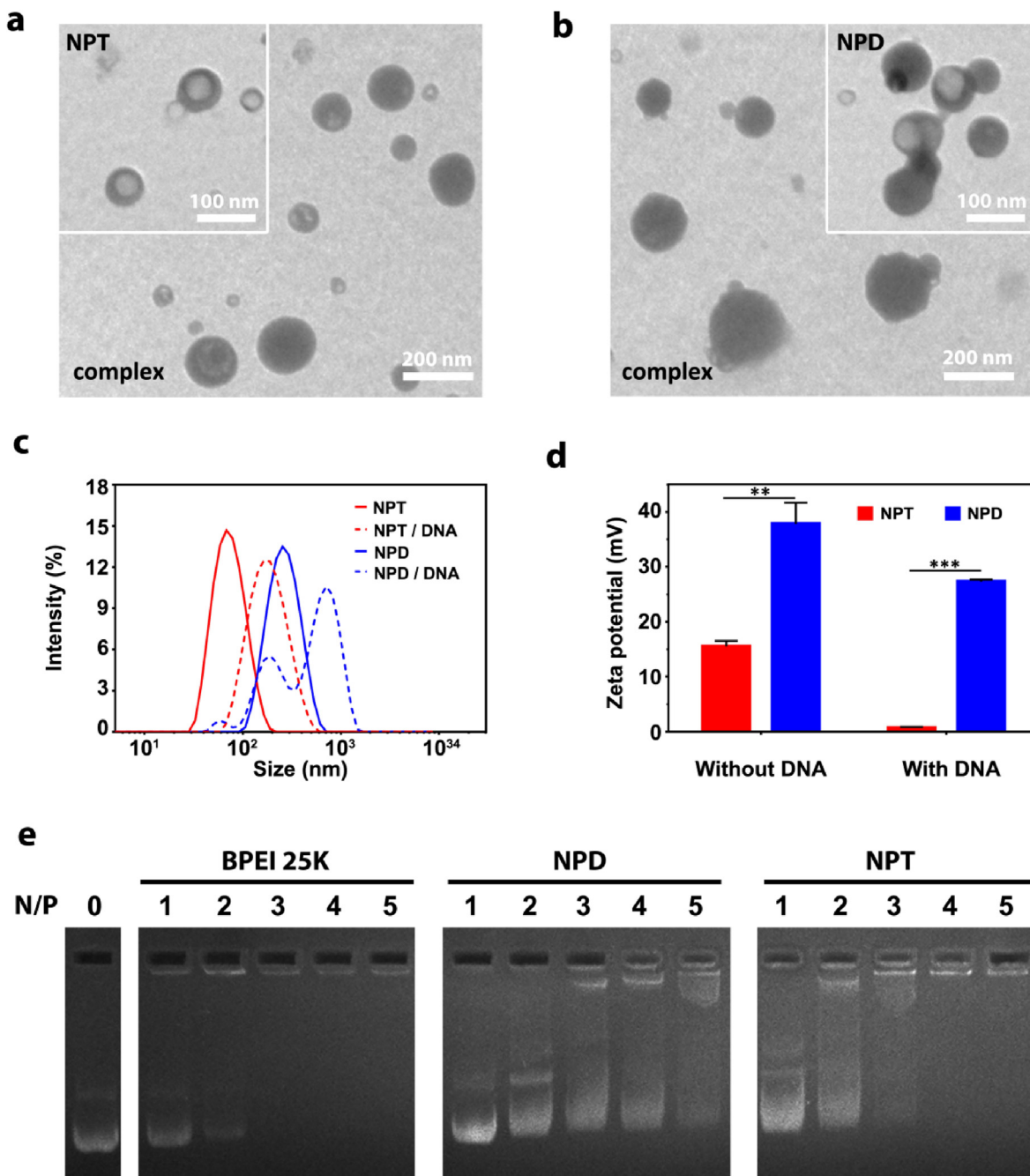


Fig. 1. Representative TEM images of (a) NPT and DNA-loaded NPT, (b) NPD and DNA-loaded NPD (N/P ratio = 10). Scale bar is shown in figures. (c) Size distribution of NPT/NPD and DNA-loaded NPT/NPD. (d) Zeta potential of NPT/NPD and DNA-loaded NPT/NPD in aqueous solution ($n = 3$; mean \pm SD). (e) DNA binding ability assay of BPEI 25 K, NPD and NPT at different N/P ratios.

(6×10^4 cells per well) were seeded on 24-well plates individually. When cell confluence reached 80%, the medium was replaced by RPMI 1640 medium containing Cy5 DNA-loaded NPT/NPD (Cy5 DNA at 1 μ g/well, N/P ratio = 10). After incubating for 1 h and 4 h, cells were digested by Trypsin and resuspended in 500 μ L PBS for flow cytometry analysis.

2.6. In vitro gene transfection efficiency

In gene transfection efficiency assay, plasmids encoding green fluorescent protein (GFP) were used as report genes. Confocal analysis and flow cytometry analysis were conducted for qualitative and quantitative investigation. For Confocal analysis, MCF-7 cells (8×10^4 cells

per well) and HeLa cells (7×10^4 cells per well) were seeded on 24-well plates individually. When cell confluence reached 70%, the old medium was replaced by RPMI 1640 medium containing pGFP-loaded NPT/NPD to incubate cells for 4 h. For anti-serum ability evaluation, 10% FBS was contained in medium. pGFP was added 2 μ g per well and N/P ratios were 5 and 10. After 4 h incubation, the medium was removed and complete medium was added to incubate for another 44 h. Stable transferred HeLa cells were seeded in 96-well plates with 8000 cells per well. After 70% cell confluence, fresh medium containing materials/siEGFR complexes were added for 4 h incubation. Then complete medium was added to incubate cells for another 44 h. Then CLSM was used for observation. For flow cytometry, MCF-7 cells (8×10^4 cells per well) and HeLa cells (7×10^4 cells per well) were

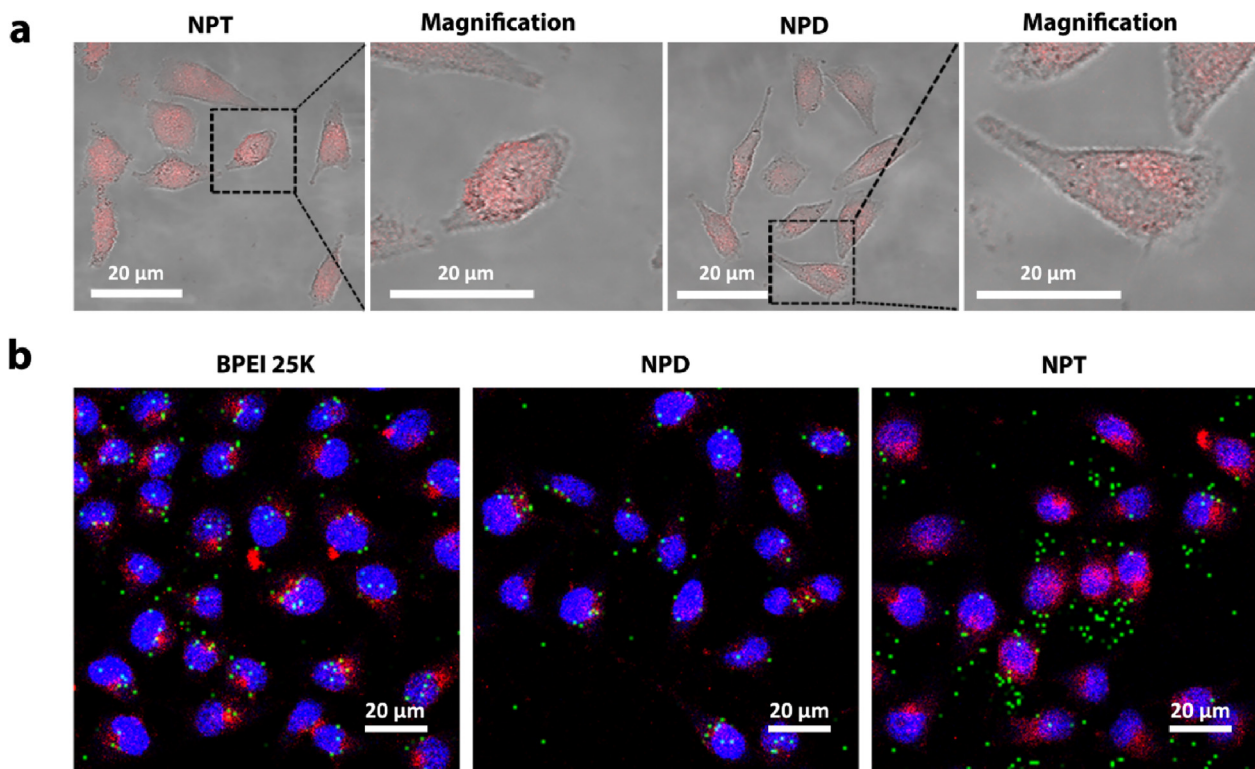


Fig. 2. (a) Confocal laser scanning microscopy (CLSM) images of live MCF-7 cells treated by NPT and NPD labeled with Rhodamine B for 1 h. Scale bar = 20 μ m. (b) CLSM images of MCF-7 cells treated with materials/Cy5 DNA complexes for 2 h. Cy5 DNA is shown in red, lysosomes are shown in green, and the cell nuclei are in blue. Scale bar = 20 μ m. (For interpretation of the references to colour in this figure legend, the reader is referred to the web version of this article.)

seeded on 24-well plates individually. When cell confluence reached 70%, the old medium was replaced by RPMI 1640 medium containing pGFP-loaded NPT/NPD to incubate cells for 4 h. Another group with 10% FBS was prepared to investigate anti-serum ability. pGFP was added 2 μ g per well and N/P ratios were 5 and 10. After 4 h incubation, the old medium was replaced by fresh complete medium to incubate for another 44 h. Then cells were digested by Trypsin and resuspended in 500 μ L PBS for flow cytometry analysis.

2.7. Cell viability assay

MCF-7 cells (1×10^4 cells/well), HeLa cells (1×10^4 cells/well) and H293 cells (1×10^4 cells/well) were incubated on 96-well plates with 100 μ L RPMI 1640 containing 10% FBS respectively. After incubation overnight, the old medium was replaced by RPMI 1640 containing NPT, NPD and BPEI 25 K at a series of concentrations (0, 5, 10, 25, 50, 100, 200 and 300 μ g/mL) respectively. After 48 h incubation, old medium was removed and cell titer-Blue reagent (10 μ L/well) was added for another 4 h incubation. Then the fluorescence intensity was measured by microplate reader (Ex/Em: 560/590 nm).

2.8. Cell apoptosis assay

For cell viability assay, MCF-7 cells was seeded on 96-well plates with 1×10^4 cells per well. After incubation overnight, the old medium was replaced by RPMI 1640 containing NPT, NPD and BPEI 25 K loading shRNA at different concentration (0, 0.5, 1.0, 1.5 and 2.0 μ g/well) respectively. After 4 h incubation, the medium was removed and complete medium was added to incubate for another 44 h. Cell titer-Blue reagent (10 μ L/well) was added for another 4 h incubation. Then the fluorescence intensity was measured by microplate reader (Ex/Em: 560/590 nm). For flow cytometry, MCF-7 cells was seeded on 24-well plates with 7×10^4 cells per well. The cells were treated with NPT,

NPD and BPEI 25 K loading shEGFR for 48 h. Then the cells were digested by Trypsin and resuspended in 500 μ L PBS. Annexin V-FITC/PI agents was added into cell suspension and placed in dark place for 15 min. The prepared samples were analyzed by flow cytometry.

2.9. Immunofluorescence assay

In this assay, MCF-7 cells were seeded on glass-bottom petri dishes with 8×10^4 cells per well and incubate overnight. Then fresh medium containing different materials (BPEI 25 K/shEGFR, NPD/shEGFR, NPT/shGFRE and NPT/shNC) was added and treated cells for 4 h. shRNA was 2 μ g/well and N/P ratio was 10. After 4 h, fresh complete medium was added to replace old medium for another 44 h. The cells was washed with PBS for 3 times and fixed with 4% formaldehyde for 30 min at 37°C. 5% BSA was used to block cells. Then cells were incubated by antiEGFR antibody overnight at 4°C and FITC conjugated antibody 2 h in dark place.

2.10. In vivo gene therapy efficiency

MCF-7 tumor bearing BALB/c nude mice were prepared for in vivo gene therapy efficiency. First, mice whose tumor grew up to 300–500 mm^3 were chose for in vivo NIR fluorescence detection. These mice were injected with Cy5-DNA-loaded NPT/NPD (Cy5 DNA of 1 mg/kg) via tail vein. The fluorescence distribution was imaged at 3 h, 6 h, 12 h and 24 h. After injecting for 24 h, mice was sacrificed, tumor and normal organs including heart, liver, spleen, lung and kidney were excised for NIR fluorescence imaging. Tumor slices and frozen sections were prepared and observed by confocal laser scanning microscope and TUNEL staining. For in vivo tumor suppression, BALB/c nude mice were injected with MCF-7 cell suspension in the right flank of each mouse. When the tumor volume reached 100 mm^3 , mice were randomly divided into 4 groups and injected with different formula-PBS, NPT, BPEI

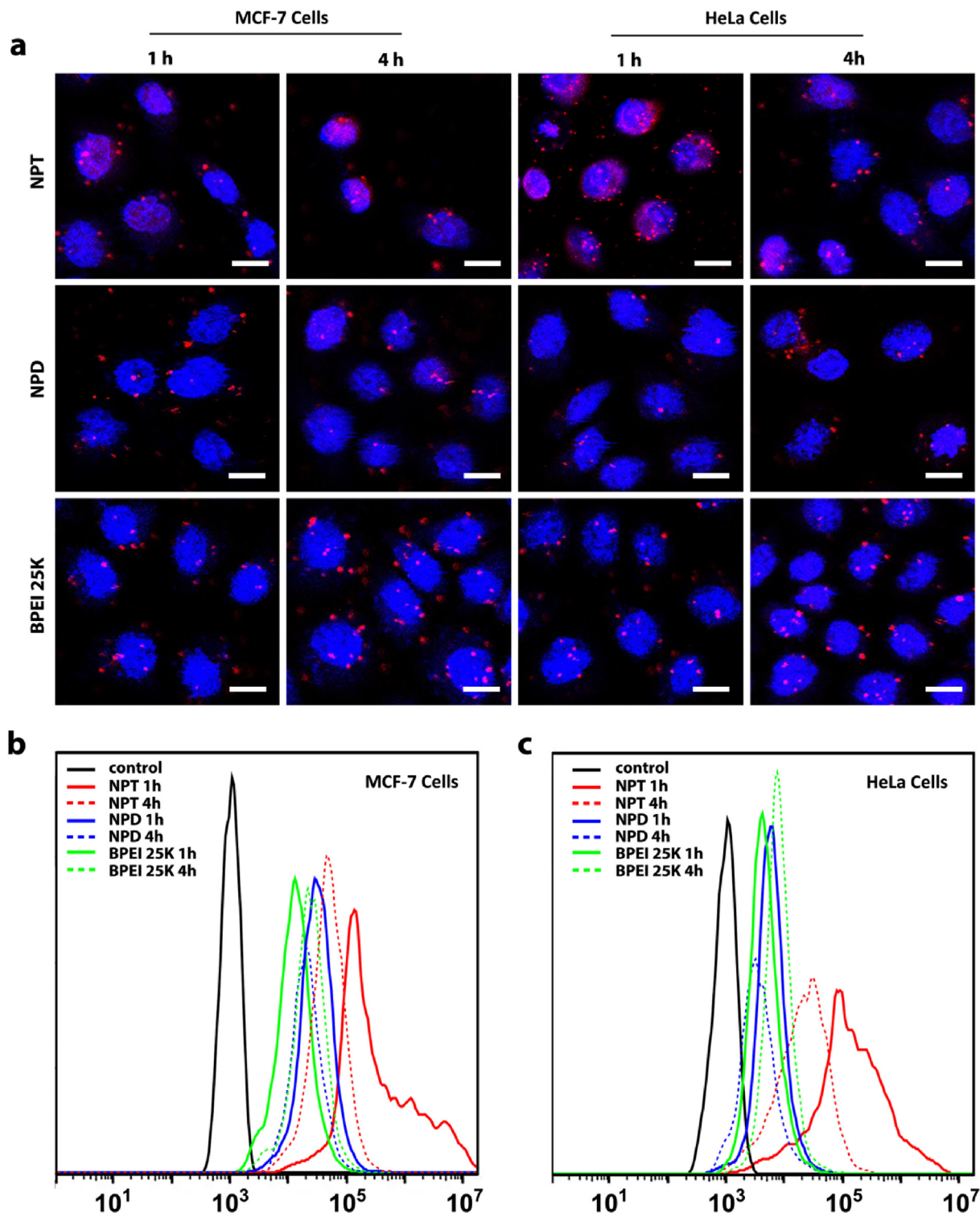


Fig. 3. (a) Representative CLSM images of MCF-7 cells and HeLa cells cultured by complexes of Cy5 DNA with NPT, NPD and BPEI 25 K at time of 1 h and 4 h. Cy5 DNA is shown in red and the cell nuclei are in blue. Scale bar: 10 μ m. Flow cytometry histograms of (b) MCF-7 cells and (c) HeLa cells transfected by complexes of Cy5 DNA with NPT, NPD and BPEI 25 K at time of 1 h and 4 h. (For interpretation of the references to colour in this figure legend, the reader is referred to the web version of this article.)

25 K/shEGFR and NPT/shEGFR (shEGFR of 1 mg/kg) via tail intravenous injection. The tumor volume was calculated using this equation: $V = 0.5 \times a \times b^2$, where a represents for length and b for width. The tumor volume and body weight of mice were measured every two days. At day 15, the mice were sacrificed and tumor and organs (heart, liver, spleen, lung and kidney) were excised for

hematoxylin and eosin (H&E) staining.

2.11. Statistics

All measurements presented are expressed as mean \pm S. D. Student's *t*-test was used to compare the statistical significance

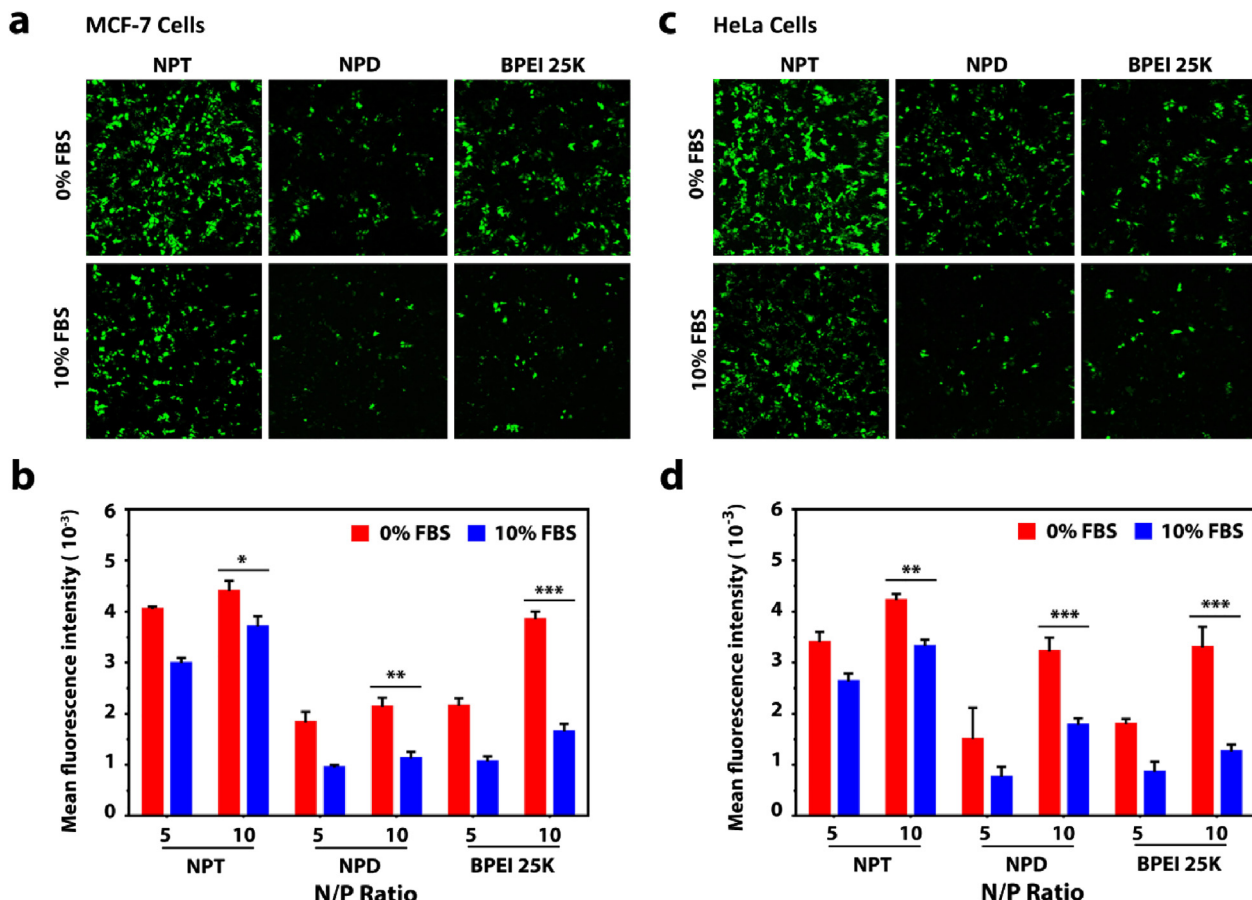


Fig. 4. In vitro gene transfection efficiency. GFP expression images of (a) MCF-7 cells and (c) HeLa cells transfected by pGFP-loaded NPT, pGFP-loaded NPD and pGFP-loaded BPEI 25 K at N/P ratio of 10. pGFP was 2 μ g/well. Mean fluorescence intensities of (b) MCF-7 cells and (d) HeLa cells transfected by different formula for 4 h and another 44 h incubation ($n = 3$; mean \pm SD).

(* $P < 0.05$, ** $P < 0.01$, *** $P < 0.001$).

3. Results and discussion

3.1. Characterization of nanoparticles and complexes.

To confirm our design, we first synthesized tri-block copolymer C₇F₁₅-Peptide-C₇F₁₅ to form NPT. Another di-block copolymer C₇F₁₅-peptide was also synthesized to form NPD as control. The detailed synthetic procedure was presented in [supporting information \(Figure S1\)](#). The structures of functional peptides were verified by HPLC and MS ([Figure S2 and S3](#)) and the ¹⁹F NMR and XPS assay demonstrated that fluorous chains were linked to the functional peptides as we designed successfully ([Figure S4 and S5](#)) [38]. TEM images showed NPT and NPD both exhibited as spherical nanoparticles with hollow cavity ([Fig. 1a and 1b](#)). The size of NPT was measured to be about 70.52 ± 1.40 nm with narrow distribution (< 0.28), while the size of NPD was about 153.7 ± 20.1 nm with higher dispersity (~ 0.4) as shown in [Fig. 1c](#). The difference between NPT and NPD could be explained that higher proportion of fluorocarbons induced more stable and compact assembly structures [37]. The superiority of fluorocarbons was further confirmed when nanoparticles complexed with DNA. We prepared DNA-loaded NPT and NPD (N/P ratio = 10) and investigated their morphologies and size distributions. As [Fig. 1c](#) showed, the size of DNA-loaded NPD increased to about 450.2 nm with poor uniformity (> 0.49). However, the size of DNA-loaded NPT was about 182.0 ± 1.7 nm with a low PDI around 0.2, which is suitable for enhanced permeability and retention (EPR) effect. The zeta potential measurement showed that NPT carried positive charges at

about + 15.5 mV. It is interesting to find that NPD exhibited much higher positive charged at about + 37.8 mV ([Fig. 1d](#)). This may be caused by the lower functional peptides density in NPT. Though NPT was lower positive charged, the bridge-like structure endowed it enhanced interaction with DNA than NPD in gel electrophoresis assay. As shown in [Fig. 1e](#), NPT could already complex DNA completely when N/P ratio reached 4, while NPD still could not completely bind DNA when N/P ratio reached 5. After complexing with DNA, the zeta potential of NPT decreased to about + 2.63 mV ([Fig. 1d](#)). The weak surface charge could help nanoparticles repel from each other and keep stable status. More importantly, the lower positive charge could decrease cationic-related toxicity and prolong the blood circulating time effectively.

3.2. Cellular uptake efficiency of NPT

Cellular uptake, as the key process regulating biology activity of genetic materials, is very important to the gene therapy [38]. In NPT, the fluorous chains linked in two ends made functional peptides forming bridge-like structures which could maximize the interaction of guanidine groups with cell membrane and definitely bring excellent cellular internalization efficiency. This property was characterized by confocal lazer scanning microscope and flow cytometry. NPT and NPD were labeled with Rhodamine B and incubated MCF-7 cells for 1 h. Though NPT carried lower positive charge than NPD, stronger red fluorescence was observed in cells incubated with NPT compared with cells incubated with NPD ([Fig. 2a](#)), which indicated the excellent internalization of NPT. Furthermore, the red fluorescence of NPT could be observed in nuclei region while NPD were distributed in cytoplasm, indicating the efficient endosomal escape ability of NPT. Then we

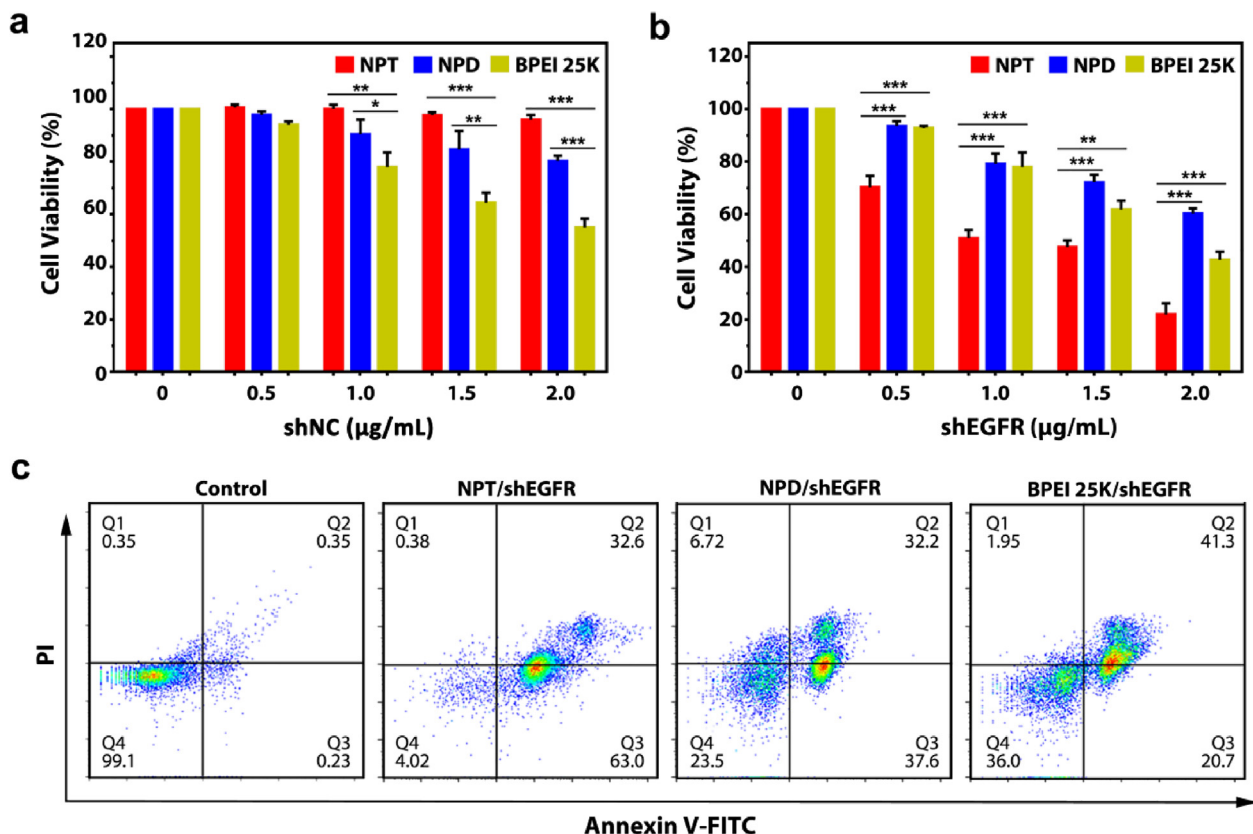


Fig. 5. In vitro gene therapy efficiency. (a) Cell viability of MCF-7 cells incubated with shNC-loaded NPT, NPD and BPEI 25 K (N/P ratio = 10) for 48 h. (b) Cell viability of MCF-7 cells incubated with shEGFR-loaded NPT, NPD and BPEI 25 K (N/P ratio = 10) for 48 h. (c) MCF-7 cell apoptosis evaluation incubated with different formulas for 48 h assessed by flow cytometry. shEGFR was 2 $\mu\text{g}/\text{well}$.

prepared Cy5 DNA-loaded NPT and Cy5 DNA-loaded NPD (N/P ratio = 10) to confirm the endosomal escaping effect after loading DNA. Commercial gene transfection material BPEI 25 K was also prepared as control. As shown in Fig. 2b, Cy5 DNA delivered by BPEI 25 K and NPD was mainly entrapped in endosome while most Cy5 DNA delivered by NPT was visible in nuclei.

In Fig. 3a, red dot could be clearly observed in cytoplasm and nuclei of MCF-7 cells, while cells incubated with NPD and BPEI 25 K showed weak fluorescence when the incubation time reached 1 h. These results further suggested the excellent cellular uptake efficiency of NPT. Furthermore, red fluorescence was most concentrated in nuclei when incubating time reached 4 h, which proved DNA was released successfully from NPT into nucleus (Fig. 3a). The quantitative measurement via flow cytometry showed NPT performed almost one order of magnitude higher cellular uptake efficiency than NPD and BPEI 25 K at 1 h (Fig. 3b). The apparent DNA fluorescence signal decreasing in NPT group was attributed to efficient and fast (enter nuclei in 2 h) releasing. After DNA entering the nuclei, consumption of DNA caused fluorescence intensity decreasing. The similar tendency was showed up in HeLa cells and confirmed the significant gene transport ability of NPT (Fig. 3a and 3c).

3.3. In vitro gene transfection efficiency.

Since NPT could transport genes into cytoplasm and released them into nuclei efficiently, NPT was expected to have high gene transfection efficiency. In this study, plasmids encoding green fluorescence protein (GFP) were used as report genes to characterize the gene transfection efficiency. Still, NPD and BPEI 25 K were conducted for control. These three kinds of materials were complexed with GFP-plasmids (pGFP) at N/P ratio of 5 and 10 and transfected MCF-7/HeLa cells with 0% or

10% FBS. Representative GFP expression images in Fig. 4a showed that in MCF-7 cells, NPT exhibited significantly highest GFP gene transfection efficiency than NPD and BPEI 25 K did. At N/P ratio of 5, NPT already got similar gene transfection efficiency with BPEI 25 K at N/P ratio of 10. The same results were also observed in flow cytometry data (Fig. 4b). Results in HeLa cells suggested the superior transfection efficiency of NPT further (Fig. 4c and 4d). At the same time, the expression of GFP in stable transferred HeLa cells was efficiently inhibited by NPT/siEGFR (Figure S6). To evaluate ability against serum, same GFP transfection experiments were conducted in 10% FBS. The gene transfection efficiency still remained a high level whereas efficiency of BPEI 25 K was significantly decreased (Fig. 4). The results verified the great anti-serum ability of NPT. Compared with NPD, higher proportion of fluorous compounds conferred NPT stability against protein due to their special bioinert. At the same time low surface charge of NPT also helped reduce the interaction with serum protein. The anti-serum property of NPT guaranteed prolonged circulating time in blood.

3.4. Cell apoptosis assay.

Afterwards, the cell apoptosis assay was conducted to evaluate in vitro gene therapy efficiency. First we examined the cytotoxicity of NPT, NPD and BPEI 25 K individually. In cell viability assay, BPEI 25 K exhibited obvious cytotoxicity at all three types of cell lines (tumor cell lines: MCF-7 cells and HeLa cells; normal cell line: H293 cells) as shown in Figure S7, S8 and S9. When concentration of BPEI 25 K reached 300 $\mu\text{g}/\text{mL}$, cell viabilities of three cell lines were all < 10%, exhibiting poor biocompatibility. By contrast, NPT exhibited neglected cytotoxicity and NPD resulted in some damage due to higher positive charge. These results have proved excellent biosafety of NPT material. Then we chose shEGFR as therapeutic genetic material. Function of shEGFR

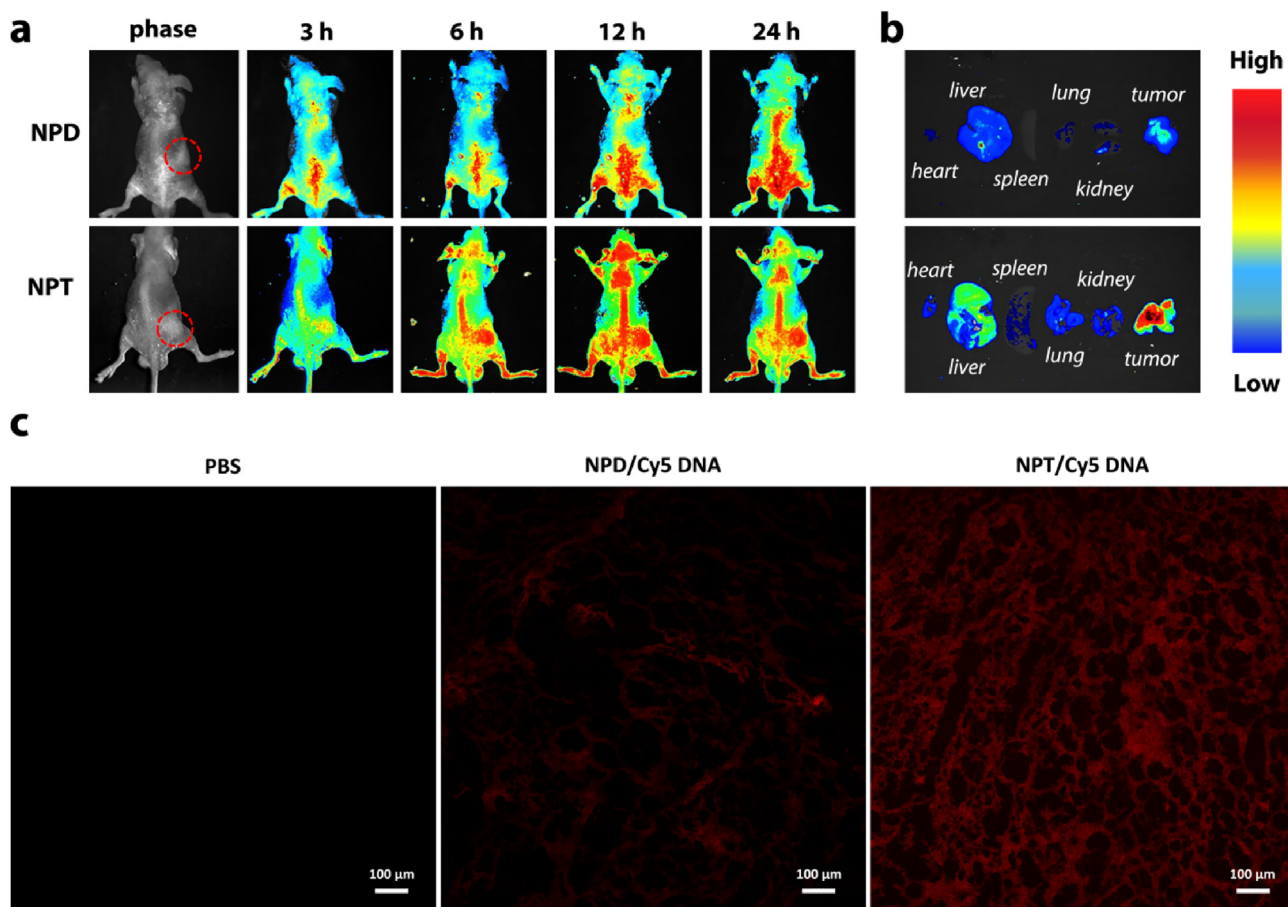


Fig. 6. In vivo distribution assay. (a) The in vivo fluorescence distribution of NPT/Cy5 DNA and NPD/Cy5 DNA in MCF-7 tumor bearing BALB/c nude mice at 3, 6, 12, and 24 h after intravenous injection. (b) The distribution of NPT/Cy5 DNA and NPD/Cy5 DNA in normal organs and tumor at 24 h. (c) Representative CLSM images of MCF-7 tumor slices treated by PBS, NPD/Cy5 DNA and NPT/Cy5 DNA. Cy5 DNA is shown in red. Scale bar: 100 μ m. (For interpretation of the references to colour in this figure legend, the reader is referred to the web version of this article.)

could down-regulate the EGFR expression, prohibit the proliferation and migration of tumor cells and lead to apoptosis eventually. The complexes of shEGFR with NPT, NPD and BPEI 25 K (N/P ratio = 10) incubated MCF-7 cells to evaluate apoptosis situation. shNC was conducted as negative control to verify the silencing specificity. As shown in **Figure S10**, the green fluorescence was obviously decreased when cells were treated by shEGFR/materials complexes indicating efficient silencing of EGFR. We could see that NPT/shEGFR induced highest apoptosis efficiency among three materials, the cell viability decreased to about 20% when the amount of shEGFR was 2 μ g/cell. The cell viability incubated with NPD and BPEI 25 K remained about 40% (**Fig. 5b**). As shown in **Fig. 5c**, NPT/shEGFR obviously caused higher MCF-7 cell apoptosis than NPD and BPEI 25 K did, which was consistent with previous results. When materials complexed with shNC, the cell viability of NPT still exceeded 90% at highest concentration. Cell viabilities of another two groups were a bit higher than groups treated by materials themselves which was attributed to the positive charge decreasing after complexing with shNC (**Fig. 5a**). These results indicate the good gene therapy efficiency of NPT/shEGFR.

3.5. In vivo anti-tumor efficiency

Since NPT exhibited great in vitro serum stability and gene therapy efficiency, we prepared MCF-7 tumor-bearing BALB/c nude mice to investigate in vivo tumor therapy effect. The mice were injected with Cy5 DNA loaded NPD and NPT respectively. As shown in **Fig. 6a**, little fluorescence signal could be detected at tumor site after injection with NPD/Cy5 DNA. Compared with NPD, obvious fluorescence signal could

be observed in tumor site at 3 h after injection with NPT/Cy5 DNA. The fluorescence signal became strongest at 12 h and still could be detected after 24 h, suggesting that NPT hold great potential to prolong blood circulating time of genetic materials. When injection time reached 24 h, the tumor and normal organs were excised and photographed to analyze the distribution of Cy5 DNA. It could be seen that NPT/Cy5 DNA mostly accumulated in tumor with the help of EPR effect. At the same time, very weak signals could be detected in normal organs which meant decreased side effects (**Fig. 6b**). The tumor slices images further illustrated the distribution in tumor of NPs (**Fig. 6c**). It is obvious that NPT could help plasmids accumulate in tumor tissue efficiently. Then in vivo antitumor efficacy was evaluated via intravenously injection of various formulations including PBS, NPT, BPEI 25 K/shEGFR and NPT/shEGFR. As shown in **Fig. 7a** and **7c**, NPT/shEGFR exhibited the greatest suppression on the growth of tumor which was remarkably better than the positive control BPEI 25 K/shEGFR. Furthermore, the data in **Fig. 7b** showed that body weight of mice injected with PBS, NPT and PEI 25 K/shEGFR decreased continuously with time. The change of body weight should be effected by tumor growth. It could be proved that the group injected with NPT/shEGFR showed no obvious change in body weight with the successful suppression of tumors. Hematoxylin and eosin (H&E) assay results (**Fig. 7d**, **Figure S11**) showed NPT/shEGFR brought about obvious damage to tumor tissues and negligible damage to normal organs. It could be observed the morphology of tumor cell treated by NPT/shEGFR was different from cells treated by PBS. The integrity was obviously damaged. As shown in **Fig. 7e**, apoptotic cells (green fluorescence) in NPT groups were more than BPEI 25 K and NPD groups. The in vivo antitumor results indicated the great

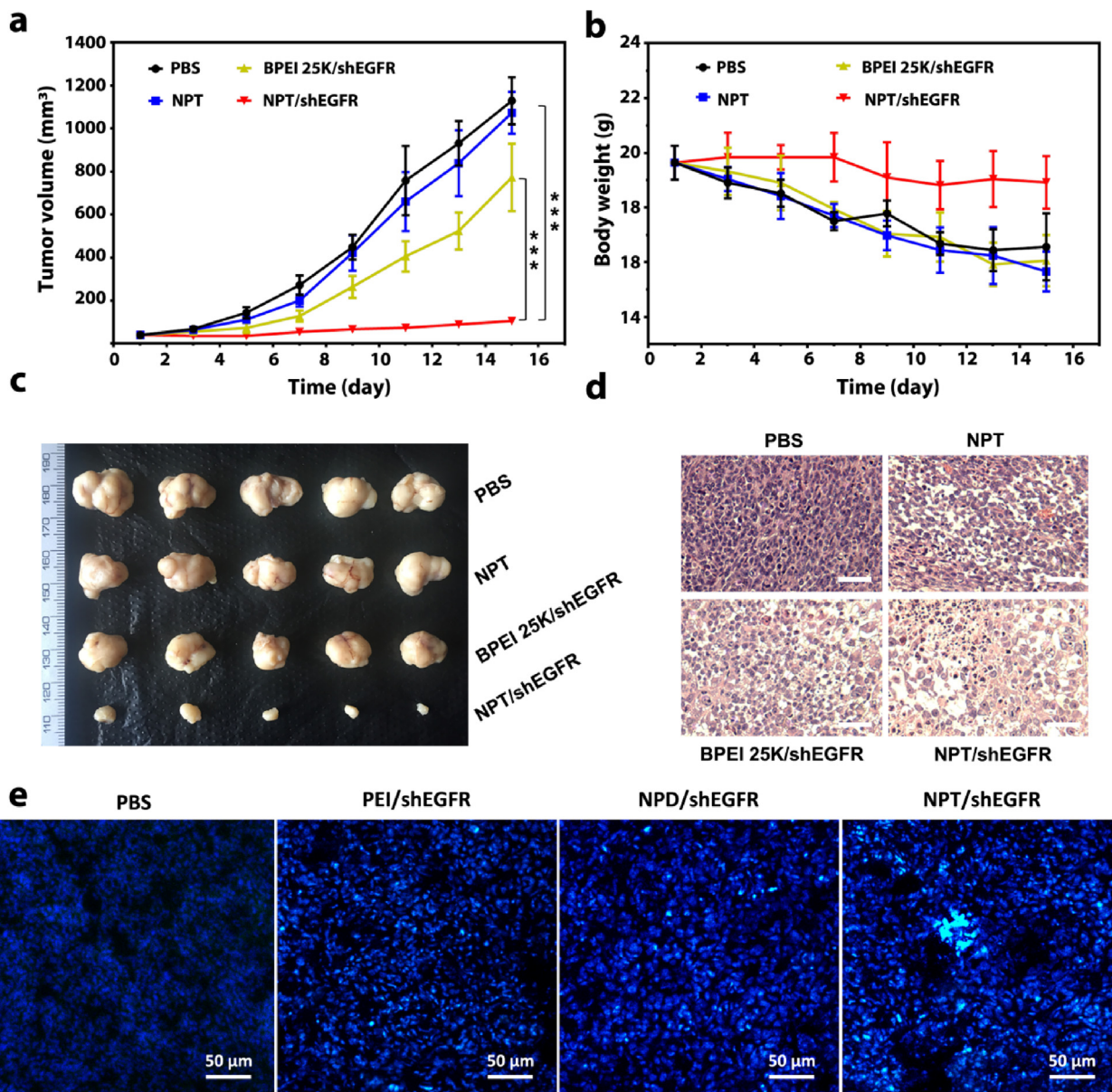


Fig. 7. In vivo tumor therapy effect. (a) The change of tumor volume in mice treated with different formula during 15 days. (b) The change of body weight in mice treated with different formula during 15 days. (c) Representative images of the tumor after different treatments. (d) Hematoxylin and eosin (H&E) staining of tumor tissues treated by different formulations. Scale bar: 50 μm . (e) TUNEL staining images of tumor tissues treated by different formulations. Apoptotic cells were shown in green. Scale bar: 50 μm . (For interpretation of the references to colour in this figure legend, the reader is referred to the web version of this article.)

potential of NPT in tumor targeting therapy.

4. Conclusions

In conclusion, we designed and synthesized a novel arginine-rich gene delivery system NPT successfully. The bridge-like structure in NPT extremely promoted the membrane contacting efficiency of arginine residues leading to great cellular uptake efficiency consequently. Meanwhile, existence of flurous chains increased the stability of whole system, conferring NPT antiserum ability. When DNA-loaded NPT entered into the cell, histidine residues in functional peptides could protonate in acid environment and induce endosome swelling, which contributed to their escaping from endosomes finally. Compared with NPD with traditional structure, NPT exhibited significant gene transfection efficiency, enhanced *in vivo* tumor accumulation and therapy effect with much lower toxicity. The systematical evaluation in this study suggested great potential of NPT in clinical application.

Declaration of Competing Interest

The authors declare that they have no known competing financial interests or personal relationships that could have appeared to influence the work reported in this paper.

Acknowledgement

The financial support from the Nation Natural Science Foundation of China (21674109 and 21603214) is acknowledged.

Appendix A. Supplementary data

Supplementary data to this article can be found online at <https://doi.org/10.1016/j.cej.2020.125171>.

References

- [1] D. Ibraheem, A. Elaissari, H. Fessi, Gene therapy and DNA delivery systems, *Int. J. Pharm.* 459 (2014) 70–83.
- [2] C.H. Jones, C.K. Chen, A. Ravikrishnan, S. Rane, B.A. Pfeifer, Overcoming nonviral gene delivery barriers: perspective and future, *Mol. Pharm.* 10 (2013) 4082–4098.
- [3] L. Naldini, Gene therapy returns to centre stage, *Nature* 526 (2015) 351–360.
- [4] M.J. Begley, C.H. Yun, C.A. Gewinner, J.M. Asara, J.L. Johnson, A.J. Coyle, M.J. Eck, I. Apostolou, L.C. Cantley, EGF-receptor specificity for phosphotyrosine-primed substrates provides signal integration with Src, *Nat. Struct. Mol. Biol.* 22 (2015) 983–990.
- [5] S.A. Khelwatty, S. Essapen, A.M. Seddon, H. Modjtahedi, Prognostic significance and targeting of HER family in colorectal cancer, *Front. Biosci.* 18 (2013) 394–421.
- [6] U. Lachelt, E. Wagner, Nucleic Acid Therapeutics Using Polyplexes: A Journey of 50 Years (and Beyond), *Chem. Rev.* 115 (2015) 11043–11078.
- [7] J. Mosquera, I. Garcia, L.M. Liz-Marzan, Cellular Uptake of Nanoparticles versus Small Molecules: A Matter of Size, *Acc. Chem. Res.* 51 (2018) 2305–2313.
- [8] J. Yang, H. Liu, X. Zhang, Design, preparation and application of nucleic acid delivery carriers, *Biotech. Adv.* 32 (2014) 804–817.
- [9] P. Kesharwani, A.K. Iyer, Recent advances in dendrimer-based nanovectors for tumor-targeted drug and gene delivery, *Drug Discov Today* 20 (2015) 536–547.
- [10] S. He, W. Fan, N. Wu, J. Zhu, Y. Miao, X. Miao, F. Li, X. Zhang, Y. Gan, Lipid-Based Liquid Crystalline Nanoparticles Facilitate Cytosolic Delivery of siRNA via Structural Transformation, *Nano Lett.* 18 (2018) 2411–2419.
- [11] W.F. Lai, W.T. Wong, Design of Polymeric Gene Carriers for Effective Intracellular Delivery, *Trends Biotechnol.* 36 (2018) 713–728.
- [12] M.S. Al-Dosari, X. Gao, Nonviral gene delivery: principle, limitations, and recent progress, *AAPS J.* 11 (2009) 671–681.
- [13] T. Lehto, K. Ezzat, M.J.A. Wood, S. El Andaloussi, Peptides for nucleic acid delivery, *Adv. Drug. Delivery Rev.* 106 (2016) 172–182.
- [14] D.M. Copolovici, K. Langel, E. Eriste, Ü. Langel, Cell-Penetrating Peptides: Design, Synthesis, and Applications, *ACS Nano* 8 (2014) 1972–1994.
- [15] S.L. Lo, S. Wang, An endosomolytic Tat peptide produced by incorporation of histidine and cysteine residues as a nonviral vector for DNA transfection, *Biomaterials* 29 (2008) 2408–2414.
- [16] I.A. Khalil, S. Kimura, Y. Sato, H. Harashima, Synergism between a cell penetrating peptide and a pH-sensitive cationic lipid in efficient gene delivery based on double-coated nanoparticles, *J. Controlled Release* 275 (2018) 107–116.
- [17] I. Nakase, T. Takeuchi, G. Tanaka, S. Futaki, Methodological and cellular aspects that govern the internalization mechanisms of arginine-rich cell-penetrating peptides, *Adv. Drug. Delivery Rev.* 60 (2008) 598–607.
- [18] P.A. Wender, W.C. Galliher, E.A. Goun, L.R. Jones, T.H. Pillow, The design of guanidinium-rich transporters and their internalization mechanisms, *Adv. Drug. Delivery Rev.* 60 (2008) 452–472.
- [19] S. Futaki, I. Nakase, Cell-Surface Interactions on Arginine-Rich Cell-Penetrating Peptides Allow for Multiplex Modes of Internalization, *Acc. Chem. Res.* 50 (2017) 2449–2456.
- [20] H. Tang, L. Yin, K.H. Kim, J. Cheng, Helical Poly(arginine) Mimics with Superior Cell-Penetrating and Molecular Transporting Properties, *Chem. Sci.* 4 (2013) 3839–3844.
- [21] Y.W. Won, P.P. Adhikary, K.S. Lim, H.J. Kim, J.K. Kim, Y.H. Kim, Oligopeptide complex for targeted non-viral gene delivery to adipocytes, *Nat. Mater.* 13 (2014) 1157–1164.
- [22] Z. Tai, X. Wang, J. Tian, Y. Gao, L. Zhang, C. Yao, X. Wu, W. Zhang, Q. Zhu, S. Gao, Biodegradable stearylated peptide with internal disulfide bonds for efficient delivery of siRNA in vitro and in vivo, *Biomacromolecules* 16 (2015) 1119–1130.
- [23] Q.U. Ain, H. Chung, J.Y. Chung, J.-H. Choi, Y.-H. Kim, Amelioration of atherosclerotic inflammation and plaques via endothelial adrenoceptor-targeted eNOS gene delivery using redox-sensitive polymer bearing L-arginine, *J. Controlled Release* 262 (2017) 72–86.
- [24] H. Li, T. Luo, R. Sheng, J. Sun, Z. Wang, A. Cao, Achieving high gene delivery performance with caveolae-mediated endocytosis pathway by (L)-arginine/(L)-histidine co-modified cationic gene carriers, *Colloids Surf. B: Biointerfaces* 148 (2016) 73–84.
- [25] J. Yoo, D. Lee, V. Gujrati, N.S. Rejinold, K.M. Lekshmi, S. Uthaman, C. Jeong, I.-K. Park, S. Jon, Y.-C. Kim, Bioreducible branched poly(modified nona-arginine) cell-penetrating peptide as a novel gene delivery platform, *J. Controlled Release* 246 (2017) 142–154.
- [26] P.A. Wender, D.J. Mitchell, K. Pattabiraman, E.T. Pelkey, L. Steinman, J.B. Rothbard, The design, synthesis, and evaluation of molecules that enable or enhance cellular uptake: Peptoid molecular transporters, *Proc. Natl. Acad. Sci. U. S. A.* 97 (2000) 13003–13008.
- [27] S. Futaki, T. Suzuki, W. Ohashi, T. Yagami, S. Tanaka, K. Ueda, Y. Sugiura, Arginine-rich peptides - An abundant source of membrane-permeable peptides having potential as carriers for intracellular protein delivery, *J. Bio. Chem.* 276 (2001) 5836–5840.
- [28] G. Lattig-Tunnemann, M. Prinz, D. Hoffmann, J. Behlke, C. Palm-Apergi, I. Morano, H.D. Herce, M.C. Cardoso, Backbone rigidity and static presentation of guanidinium groups increases cellular uptake of arginine-rich cell-penetrating peptides, *Nat. Commun.* 2 (2011) 453.
- [29] J.B. Rothbard, E. Kreider, C.L. Vandevenus, L. Wright, B.L. Wylie, P.A. Wender, Arginine-rich molecular transporters for drug delivery: Role of backbone spacing in cellular uptake, *J. Med. Chem.* 45 (2002) 3612–3618.
- [30] W. Xiao, J.Y. Xiong, S. Zhang, Y. Xiong, H.J. Zhang, H.L. Gao, Influence of ligands property and particle size of gold nanoparticles on the protein adsorption and corresponding targeting ability, *Int. J. Pharm.* 538 (2018) 105–111.
- [31] W. Xiao, H.L. Gao, The impact of protein corona on the behavior and targeting capability of nanoparticle-based delivery system, *Int. J. Pharm.* 552 (2018) 328–339.
- [32] W. Liang, J.K.W. Lam, Endosomal Escape Pathways for Non-Viral Nucleic Acid, *Delivery Systems*. (2012).
- [33] A.K. Varkouthi, M. Scholte, G. Storm, H.J. Haisma, Endosomal escape pathways for delivery of biologicals, *J. Controlled Release* 151 (2011) 220–228.
- [34] M. Wang, H. Liu, L. Li, Y. Cheng, A fluorinated dendrimer achieves excellent gene transfection efficacy at extremely low nitrogen to phosphorus ratios, *Nat. Commun.* 5 (2014) 3053.
- [35] H. Wang, Y. Wang, Y. Wang, J. Hu, T. Li, H. Liu, Q. Zhang, Y. Cheng, Self-Assembled Fluorodendrimers Combine the Features of Lipid and Polymeric Vectors in Gene Delivery, *Angew. Chem. Int. Ed.* 54 (2015) 11647–11651.
- [36] Z. Zhang, W. Shen, J. Ling, Y. Yan, J. Hu, Y. Cheng, The fluorination effect of fluoroamphiphiles in cytosolic protein delivery, *Nat. Commun.* 9 (2018) 1377.
- [37] S. Li, X. Yan, Y. Qu, W. Wang, B. Chen, X. Ma, S. Liu, X. Yu, Hydrogen-Bond Cyclization Programming of Ultrasensitive Esters and Its Application in Gene Delivery, *Chemistry* 25 (2019) 10375–10384.
- [38] M. Piest, J.F.J. Engbersen, Effects of charge density and hydrophobicity: Acetylation versus benzoylation of amino butyl SS-PAAS for gene delivery, *J. Controlled Release* 148 (2010) E92–E94.